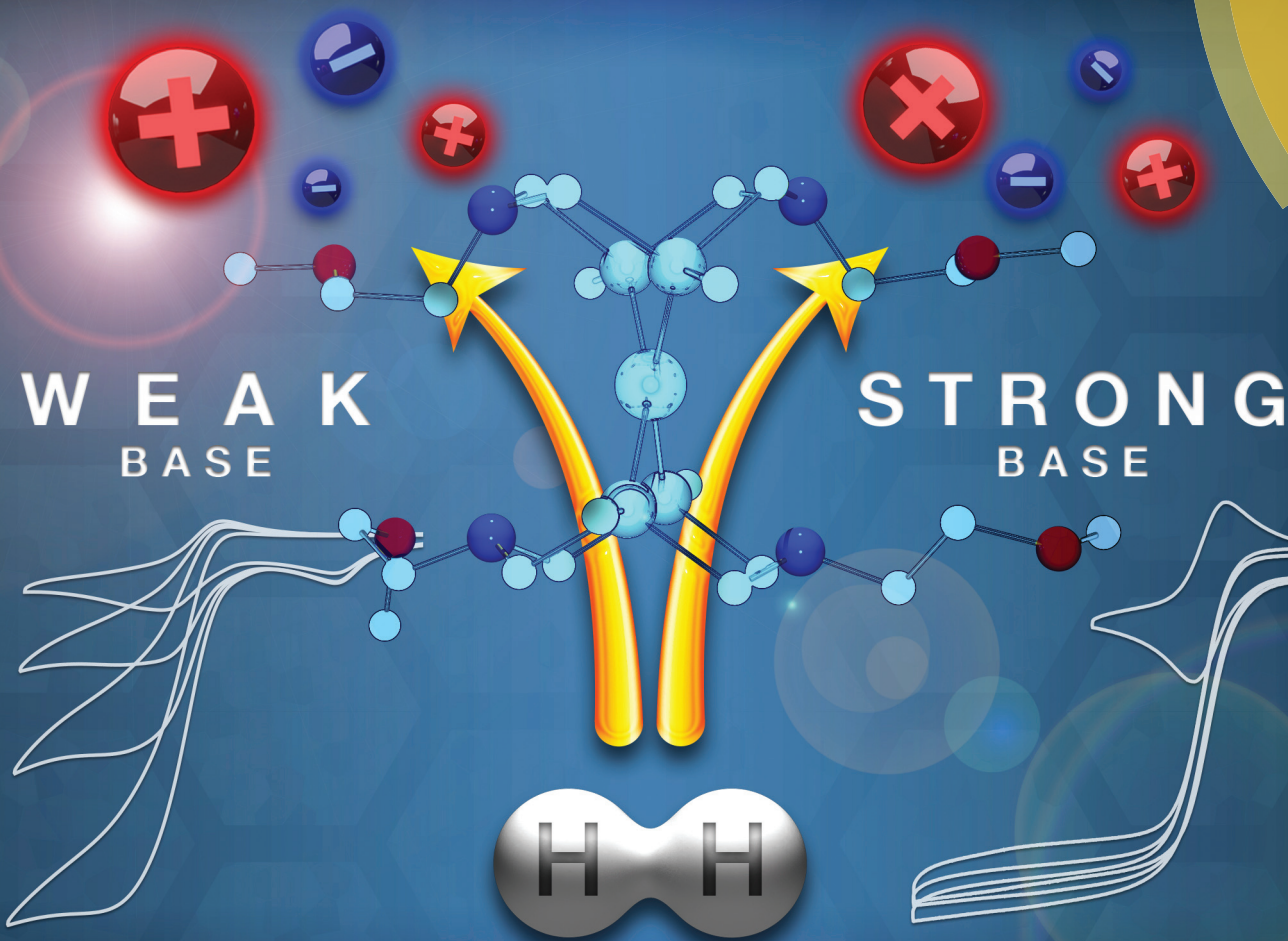


Dalton Transactions

An international journal of inorganic chemistry
www.rsc.org/dalton



ISSN 1477-9226



COVER ARTICLE

Helm *et al.*

Controlling proton movement: electrocatalytic oxidation of hydrogen by a nickel(II) complex containing proton relays in the second and outer coordination spheres

Controlling proton movement: electrocatalytic oxidation of hydrogen by a nickel(II) complex containing proton relays in the second and outer coordination spheres†

Cite this: *Dalton Trans.*, 2014, **43**, 2744

Parthapratim Das, Ming-Hsun Ho, Molly O'Hagan, Wendy J. Shaw, R. Morris Bullock, Simone Raugei and Monte L. Helm*

A nickel bis(diphosphine) complex containing proton relays in the second and outer coordination spheres, $\text{Ni}(\text{P}^{\text{Cy}}_2\text{N}^{(\text{CH}_2)_2\text{OMe}})_2$, ($\text{P}^{\text{Cy}}_2\text{N}^{(\text{CH}_2)_2\text{OMe}} = 1,5\text{-di(methoxyethyl)-3,7-dicyclohexyl-1,5-diaza-3,7-diphosphacyclooctane}$), is an electrocatalyst for hydrogen oxidation. The addition of hydrogen to the Ni(II) complex results in rapid formation of three isomers of the doubly protonated Ni(0) complex, $[\text{Ni}(\text{P}^{\text{Cy}}_2\text{N}^{(\text{CH}_2)_2\text{OMe}}_2\text{H})_2]^{2+}$. The three isomers show fast interconversion at 40 °C, unique to this complex in this class of catalysts. Under conditions of 1.0 atm H_2 using H_2O as a base, catalytic oxidation proceeds at a turnover frequency of 5 s^{-1} and an overpotential of 720 mV, as determined from the potential at half of the catalytic current. Compared to the previously reported $\text{Ni}(\text{P}^{\text{Cy}}_2\text{N}^{\text{Bn}})_2$ complex, the new complex operates at a faster rate and at a lower overpotential.

Received 30th October 2013,
Accepted 24th November 2013

DOI: 10.1039/c3dt53074d

www.rsc.org/dalton

Introduction

Obtaining energy from renewable sources such as wind, solar and biomass is necessary to reduce our dependence on fossil fuels. Because of the intermittent nature of the generation of energy from solar and wind, there is a need to store energy during times of high production, so it can be used at times of high demand. Platinum is currently used as a catalyst in fuel cells for hydrogen oxidation (energy production). Due to the high cost and low abundance of platinum, catalysts based on abundant, inexpensive metals are attractive to facilitate more widespread use of renewable fuels.¹ Transition metal molecular electrocatalysts based on Ni and Co have been developed for hydrogen production, and incorporation of pendant amines functioning as proton relays are beneficial for increasing efficiency and turnover frequencies.^{2,3} There have also been recent reports of incorporating additional pendant groups in the outer coordination sphere of nickel catalysts, resulting in significant rate enhancements for hydrogen production.^{4,5}

Compared to molecular electrocatalysts that produce hydrogen, there are fewer examples of molecular electrocatalysts for

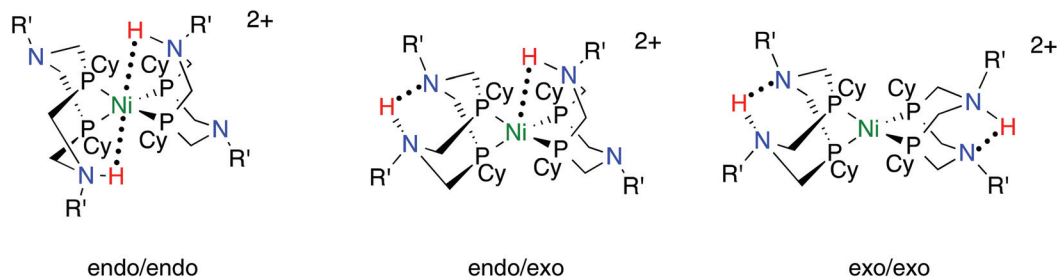
the reverse reaction, oxidation of hydrogen.^{6–13} We have found that $[\text{Ni}(\text{P}^{\text{Cy}}_2\text{N}^{\text{R}'})_2]^{2+}$ ($\text{R}' = \text{alkyl}$) are electrocatalysts for oxidation of H_2 .^{8–11} Experimental and computational data indicate that removal of protons from the catalyst by an exogenous base is a potential rate-limiting step in the mechanism for electrocatalytic oxidation of H_2 .¹⁴ Recent studies have shown that exogenous bases accelerate the isomerization between the three isomers of the Ni(0) complex $[\text{Ni}(\text{P}^{\text{Cy}}_2\text{N}^{\text{Bn}})_2]^{2+}$ (e.g. Scheme 1) that results from addition of H_2 to $[\text{Ni}(\text{P}^{\text{Cy}}_2\text{N}^{\text{Bn}})_2]^{2+}$, indicating the rates of proton movement to and from the metal complex can be influenced.¹⁴ Recent reports of the $[\text{Ni}(\text{P}^{\text{Cy}}_2\text{N}^{(3\text{-pyridazyl)methyl}})_2]^{2+}$ complex illustrated that the inclusion of an additional proton relay in the outer coordination sphere of the complex facilitates rapid proton transfer between the doubly protonated isomers and lowers the overpotential for catalysis.⁹ This work illustrates that accelerated proton movement to and from the primary and secondary coordination spheres of the metal complex can be controlled by the ligand design and influence catalyst efficiency. Although rapid proton movement was observed in $[\text{Ni}(\text{P}^{\text{Cy}}_2\text{N}^{(3\text{-pyridazyl)methyl}})_2]^{2+}$, rates of catalysis were significantly inhibited, which was thought to be due to competitive binding of the pyridazyl group with H_2 to the Ni(II) center during catalysis.⁹

In an effort to facilitate proton movement and removal from both the second and outer coordination spheres of the catalyst without limiting the rate, we designed a new $[\text{Ni}(\text{P}^{\text{R}}_2\text{N}^{\text{R}'})_2]^{2+}$ complex with additional relays in the outer coordination

Center for Molecular Electrocatalysis, Physical Sciences Division, Pacific Northwest National Laboratory, P.O. Box 999, K2-57, Richland 99352, Washington, USA.

E-mail: monte.helm@pnnl.gov

† Electronic supplementary information (ESI) available. CCDC 969326. For ESI and crystallographic data in CIF or other electronic format see DOI: 10.1039/c3dt53074d



Scheme 1 The three doubly protonated Ni(0) isomers of $[\text{Ni}(\text{P}^{\text{Cy}}_2\text{N}^{\text{R}'_2}\text{H})_2]^{2+}$.

sphere that would not competitively bind with H_2 . We report a new nickel complex bearing a methoxyethyl group appended on the pendant amine that resides in the outer coordination sphere of the compound. The three Ni(0) doubly protonated isomers resulting from H_2 addition (e.g. Scheme 1) undergo rapid interconversion, providing mechanistic insight into proton movement relevant to catalysis. Additionally, the interaction of the methoxyethyl groups with the pendant amine results in a hydrogen oxidation catalyst that can operate at both a lower overpotential and a faster rate than the $[\text{Ni}(\text{P}^{\text{Cy}}_2\text{N}^{\text{Bn}_2}\text{H})_2]^{2+}$ complex using water as an exogenous base. Importantly, this demonstrates our ability to control both rates and overpotentials through a combination of modifying the functionality of the second and outer coordination spheres.

Results

Synthesis and characterization of $\text{Ni}(\text{P}^{\text{Cy}}_2\text{N}^{(\text{CH}_2)_2\text{OMe}})_2$ and $[\text{Ni}(\text{P}^{\text{Cy}}_2\text{N}^{(\text{CH}_2)_2\text{OMe}})_2](\text{BF}_4)_2$

The cyclic diphosphine ligand $\text{P}^{\text{Cy}}_2\text{N}^{(\text{CH}_2)_2\text{OMe}}_2$ was synthesized by the condensation of bis(hydroxymethyl)cyclohexylphosphine, $\text{CyP}(\text{CH}_2\text{OH})_2$, with methoxyethylamine ($\text{MeOCH}_2\text{CH}_2\text{NH}_2$), as characterized by $^{31}\text{P}\{^1\text{H}\}$ NMR spectroscopy (eqn (1)). Attempts to isolate pure $\text{P}^{\text{Cy}}_2\text{N}^{(\text{CH}_2)_2\text{OMe}}_2$ ligand from the reaction mixture proved unsuccessful, so the ligand was generated *in situ* and reacted with $[\text{Ni}(\text{CH}_3\text{CN})_6](\text{BF}_4)_2$ to form $[\text{Ni}(\text{P}^{\text{Cy}}_2\text{N}^{(\text{CH}_2)_2\text{OMe}}_2)_2]^{2+}$. Isolation of the pure Ni(II) complex from the reaction mixture was not accomplished, however, after reduction of the Ni(II) complex with H_2 and deprotonation with tetramethylguanidine (TMG), the pure Ni(0) complex $\text{Ni}(\text{P}^{\text{Cy}}_2\text{N}^{(\text{CH}_2)_2\text{OMe}}_2)_2$ precipitated from the reaction mixture (eqn (2)). Oxidation of the Ni(0) species with two equivalents of $(\text{Cp}^*\text{Fe})(\text{BF}_4)$ ($\text{Cp}^* = \eta^5\text{-C}_5\text{Me}_5$) resulted in formation and isolation of the pure Ni(II) complex (eqn (3)); both the Ni(0) and Ni(II) species were fully characterized. An X-ray diffraction study of $[\text{Ni}(\text{P}^{\text{Cy}}_2\text{N}^{(\text{CH}_2)_2\text{OMe}}_2)_2]^{2+}$ indicates the complex has a distorted square planar geometry around the Ni(II) center (Fig. 1), as previously observed in other structurally characterized $[\text{Ni}(\text{P}^{\text{R}'_2}\text{N}^{\text{R}'_2})_2]^{2+}$ complexes.^{8,10}

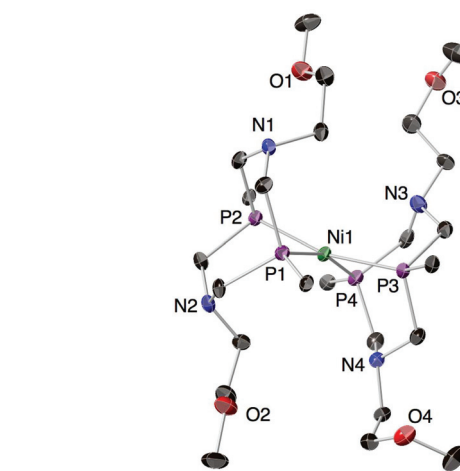
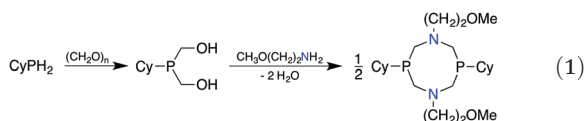
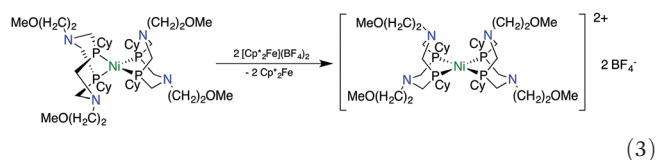
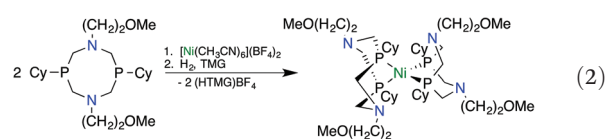


Fig. 1 X-ray crystal structure of $[\text{Ni}(\text{P}^{\text{Cy}}_2\text{N}^{(\text{CH}_2)_2\text{OMe}}_2)](\text{BF}_4)_2 \cdot 2\text{CH}_3\text{CN}$. The BF_4^- counterions, CH_3CN solvent molecules and H atoms have been omitted for clarity. Only the carbon attached to the phosphorus atom of the cyclohexyl groups is shown for clarity. Thermal ellipsoids are shown at the 50% probability level.

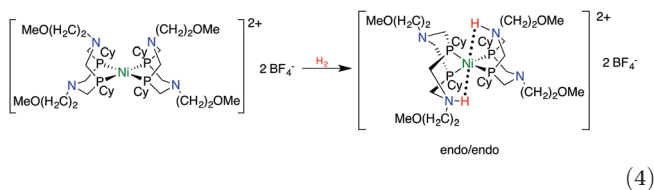


X-ray quality crystals of $[\text{Ni}(\text{P}^{\text{Cy}}_2\text{N}^{(\text{CH}_2)_2\text{OMe}}_2)](\text{BF}_4)_2$ were grown by slow diffusion of Et_2O into a saturated CH_3CN solution of the complex. The $[\text{Ni}(\text{P}^{\text{Cy}}_2\text{N}^{(\text{CH}_2)_2\text{OMe}}_2)](\text{BF}_4)_2$ complex crystallizes with two non-coordinating CH_3CN molecules per unit cell, and no close contacts are observed between the BF_4^- anions and the $[\text{Ni}(\text{P}^{\text{Cy}}_2\text{N}^{(\text{CH}_2)_2\text{OMe}}_2)]^{2+}$ cation (Fig. 1). The structure shows a distorted square planar geometry with all four Ni–P bond distances nearly equal, ranging from 2.20–2.24 Å. The P–Ni–P bond angle for each of the diphosphine ligands averages 82.2° , comparable to the 80.6° P–Ni–P angle observed in the previously reported $[\text{Ni}(\text{P}^{\text{Cy}}_2\text{N}^{(\text{tBu})_2})_2]^{2+}$ complex.⁷ The dihedral angle between the two planes defined

by the two phosphorus atoms of the bidentate P_2N_2 ligand and Ni atom is $25.59(3)^\circ$, slightly larger than the 22.53° dihedral angle reported for $[\text{Ni}(\text{P}^{\text{Cy}}_2\text{N}^{\text{tBu}}_2)_2]^{2+}$.⁷ All four of the six-membered rings formed upon coordination of the $\text{P}^{\text{Cy}}_2\text{N}^{\text{CH}_2\text{CH}_2\text{OMe}}_2$ ligands to the Ni center are in a boat conformation, as also seen in the four-coordinate structures of $[\text{Ni}(\text{P}^{\text{Cy}}_2\text{N}^{\text{Bn}}_2)_2]^{2+}$ and $[\text{Ni}(\text{P}^{\text{Cy}}_2\text{N}^{\text{tBu}}_2)_2]^{2+}$.^{7,10} Complete crystallographic information along with bond distances and angles for $[\text{Ni}(\text{P}^{\text{Cy}}_2\text{N}^{\text{(CH}_2)_2\text{OMe}}_2)_2]^{2+}(\text{BF}_4)_2$ is contained in the ESI†

Addition of H_2 to $[\text{Ni}(\text{P}^{\text{Cy}}_2\text{N}^{\text{(CH}_2)_2\text{OMe}}_2)_2]^{2+}$

Room temperature addition of H_2 (1 atm) to an acetonitrile solution of $[\text{Ni}(\text{P}^{\text{Cy}}_2\text{N}^{\text{(CH}_2)_2\text{OMe}}_2)_2]^{2+}$ leads to a color change from red to yellow indicating formation of the doubly protonated Ni(0) complex, $[\text{Ni}(\text{P}^{\text{Cy}}_2\text{N}^{\text{(CH}_2)_2\text{OMe}}_2\text{H})_2]^{2+}$, with protons in an *endo/endo* position (eqn (4)), as previously observed for other $[\text{Ni}(\text{P}^{\text{R}}_2\text{N}^{\text{R}'_2})_2]^{2+}$ catalysts for oxidation of H_2 .^{8,10} The doubly protonated $[\text{Ni}(\text{P}^{\text{Cy}}_2\text{N}^{\text{(CH}_2)_2\text{OMe}}_2\text{H})_2]^{2+}$ complex undergoes isomerization at room temperature to form an equilibrium distribution of 10% *endo/endo*, 40% *endo/exo* and 50% *exo/exo* isomers (*i.e.* Scheme 1) in the time it takes to prepare the sample (*i.e.* <15 min). The three isomers were identified by their distinct $^{31}\text{P}\{^1\text{H}\}$ NMR spectrum (Fig. S1 in the ESI†), as previously observed and reported for $[\text{Ni}(\text{P}^{\text{Cy}}_2\text{N}^{\text{Bn}}_2\text{H})_2]^{2+}$.¹⁵ Phosphorus-31 EXSY experiments carried out at 40°C (Fig. S2 in the ESI†) show strong exchange cross-peaks between both the *endo/endo* and *endo/exo* isomers and the *endo/exo* and *exo/exo* isomers at mixing times as short as 0.1 s, indicating that all three isomers are in rapid exchange. At 25°C , only the exchange peaks between the *endo/endo* and *endo/exo* isomers are observed, indicating slower exchange.



The rate of isomerization was further investigated by monitoring the time to reach equilibrium by $^{31}\text{P}\{^1\text{H}\}$ NMR spectroscopy at 0°C as a function of catalyst concentration (Fig. S3 in the ESI†). The resulting equilibrium concentrations as measured by the integration of the $^{31}\text{P}\{^1\text{H}\}$ NMR spectra of each isomer are identical to those obtained at room temperature. The time necessary to reach the equilibrium concentration of the *exo/exo* isomer at three catalyst concentrations showed no dependence on the catalyst concentration (Fig. 2), indicating the rate limiting step for this isomerization process is likely an intramolecular proton transfer process.

Electrochemical measurements

An equal stoichiometric mixture of the Ni(II) complex $[\text{Ni}(\text{P}^{\text{Cy}}_2\text{N}^{\text{(CH}_2)_2\text{OMe}}_2)_2]^{2+}$ and the Ni(0) complex $[\text{Ni}(\text{P}^{\text{Cy}}_2\text{N}^{\text{(CH}_2)_2\text{OMe}}_2)_2]^{2+}$ cleanly comproportionates to the Ni(I) $[\text{Ni}(\text{P}^{\text{Cy}}_2\text{N}^{\text{(CH}_2)_2\text{OMe}}_2)]^+$ complex. The cyclic voltammogram of $[\text{Ni}(\text{P}^{\text{Cy}}_2\text{N}^{\text{(CH}_2)_2\text{OMe}}_2)]^+$ (Fig. 3) shows two one-electron reversible redox couples,

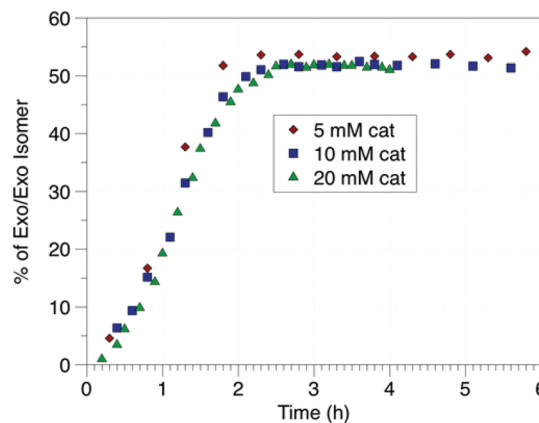


Fig. 2 Plot of the formation of the *exo/exo* isomer as a function of time at 0°C in CH_3CN at different $[\text{Ni}(\text{P}^{\text{Cy}}_2\text{N}^{\text{(CH}_2)_2\text{OMe}}_2)_2]^{2+}$ concentrations. This data shows that proton movement from *endo* to *exo* does not depend upon catalyst concentration.

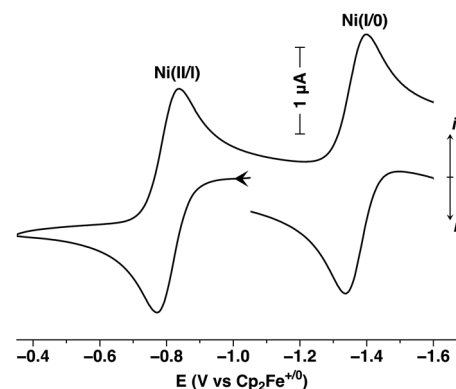


Fig. 3 Cyclic voltammogram of 1.0 mM $[\text{Ni}(\text{P}^{\text{Cy}}_2\text{N}^{\text{(CH}_2)_2\text{OMe}}_2)](\text{BF}_4)$ in 0.20 M $[\text{Bu}_4\text{N}][\text{PF}_6]-\text{CH}_3\text{CN}$. Conditions: 1 mm glassy-carbon working electrode; scan rate 0.05 V s^{-1} at 25°C .

with observed $E_{1/2}$ values (reported as the average of the potentials of the maximum cathodic and anodic current) at -0.81 V (Ni^{II/I} couple) and -1.37 V (Ni^{I/0} couple) vs. the ferrocene/ferrocene ($\text{Cp}_2\text{Fe}^{+/0}$) couple. A plot of either the anodic (i_p) or cathodic peak current of the Ni(II/I) couple vs. the square root of the scan rate shows a linear correlation, implying diffusion-controlled electrochemical events. The difference in the potential of cathodic and anodic peak potentials (ΔE_p) at a scan rate of 0.05 V s^{-1} for these processes is measured to be 63–68 mV, indicating one-electron processes in both couples. Cyclic voltammograms of the Ni(II) complex $[\text{Ni}(\text{P}^{\text{Cy}}_2\text{N}^{\text{(CH}_2)_2\text{OMe}}_2)_2]^{2+}$ and the Ni(0) complex $[\text{Ni}(\text{P}^{\text{Cy}}_2\text{N}^{\text{(CH}_2)_2\text{OMe}}_2)]^{2+}$ complexes give the same results.

Oxidation of the Ni(I) complex $[\text{Ni}(\text{P}^{\text{Cy}}_2\text{N}^{\text{(CH}_2)_2\text{OMe}}_2)]^+$ complex in the presence of H_2 results in its addition to the Ni(II) complex and formation of the *endo/endo* isomer, allowing for its electrochemical characterization (Fig. 4, blue). Electrochemical analysis of equilibrated mixtures containing all three doubly protonated Ni(0) isomers of $[\text{Ni}(\text{P}^{\text{Cy}}_2\text{N}^{\text{(CH}_2)_2\text{OMe}}_2\text{H})_2]^{2+}$ allows for the electrochemical assignment of the *exo/exo* and

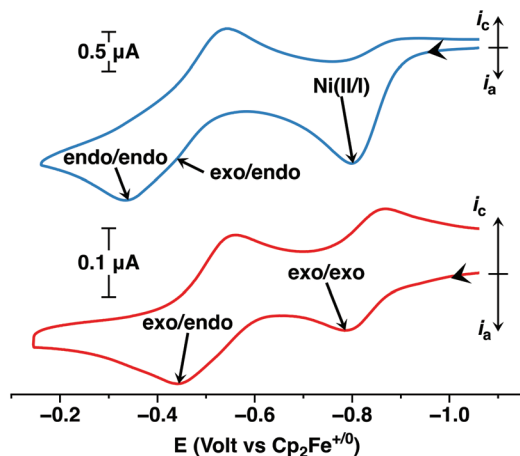


Fig. 4 Cyclic voltammograms of (red) an equilibrated mixture of 0.5 mM $[\text{Ni}(\text{P}^{\text{Cy}}_2\text{N}(\text{CH}_2)_2\text{OMe}_2)_2]^{2+}$ and (blue) 1.0 mM $[\text{Ni}(\text{P}^{\text{Cy}}_2\text{N}(\text{CH}_2)_2\text{OMe}_2)_2]^{2+}$ in the presence of 1 atm H_2 . Conditions: 0.20 M $[\text{Bu}_4\text{N}][\text{PF}_6]-\text{CH}_3\text{CN}$; 1 mm glassy-carbon working electrode; scan rate 0.05 V s^{-1} at 25°C .

Table 1 Experimental (and computational) $\text{p}K_a$ values and electrochemical potentials (V) for $\text{Ni}(\text{P}^{\text{Cy}}_2\text{N}(\text{CH}_2)_2\text{OMe}_2)_2$ and the doubly protonated $\text{Ni}(\text{O})$ isomers of $[\text{Ni}(\text{P}^{\text{Cy}}_2\text{N}(\text{CH}_2)_2\text{OMe}_2\text{H})_2]^{2+}$ in CH_3CN . Redox potentials are referenced to the $\text{Cp}_2\text{Fe}^{+/0}$ couple. The electrochemical potentials for $\text{Ni}(\text{P}^{\text{Cy}}_2\text{N}(\text{CH}_2)_2\text{OMe}_2)_2$ are half-peak potentials for the reversible waves. The electrochemical potentials for the doubly protonated $\text{Ni}(\text{O})$ isomers of $[\text{Ni}(\text{P}^{\text{Cy}}_2\text{N}(\text{CH}_2)_2\text{OMe}_2\text{H})_2]^{2+}$ are peak potentials of the irreversible waves

Compound (isomer)	$\text{p}K_a$	$\text{Ni}(\text{I}/\text{I})$	$\text{Ni}(\text{II}/\text{I})$
$\text{Ni}(\text{P}^{\text{Cy}}_2\text{N}(\text{CH}_2)_2\text{OMe}_2)_2^+$	—	-1.37	-0.81
$[\text{Ni}(\text{P}^{\text{Cy}}_2\text{N}(\text{CH}_2)_2\text{OMe}_2\text{H})_2]^{2+}$ (endo/endo)	15.1 (15.3)	-0.33 (-0.25)	—
$[\text{Ni}(\text{P}^{\text{Cy}}_2\text{N}(\text{CH}_2)_2\text{OMe}_2\text{H})_2]^{2+}$ (endo/exo)	15.2 (15.4)	-0.43 (-0.33)	—
$[\text{Ni}(\text{P}^{\text{Cy}}_2\text{N}(\text{CH}_2)_2\text{OMe}_2\text{H})_2]^{2+}$ (exo/exo)	15.4 (15.6)	-0.79 (-0.61)	—

endo/exo isomers (Fig. 4, red). Peak potentials for the three doubly protonated $\text{Ni}(\text{O})$ isomers of $[\text{Ni}(\text{P}^{\text{Cy}}_2\text{N}(\text{CH}_2)_2\text{OMe}_2\text{H})_2]^{2+}$ are reported in Table 1.

Electrocatalytic oxidation of H_2

Standard conditions for catalytic electrochemical measurements employed a 1 mM solution of the Ni complex dissolved in a 0.2 M $[\text{Bu}_4\text{N}][\text{PF}_6]-\text{CH}_3\text{CN}$ solution, 1 atm of H_2 and subsequent additions of an exogenous base to remove protons. Catalytic H_2 oxidation was identified by an increase in the anodic peak current, i_{cat} (determined at the point where the wave first plateaus (Fig. S4 in the ESI[†]). The use of NET_3 ($\text{p}K_a$ $[\text{HNET}_3]^+ = 18.82$ in CH_3CN), $^t\text{BuNH}_2$ ($\text{p}K_a$ $[\text{BuNH}_3]^+ = 18.14$ in CH_3CN), $^n\text{BuNH}_2$ ($\text{p}K_a$ $[\text{BuNH}_3]^+ = 18.26$ in CH_3CN) or H_2O ($\text{p}K_a$ $[\text{H}_3\text{O}]^+ = 2.2$ in CH_3CN) as the exogenous base all result in significant current enhancements and catalytic wave shapes, establishing catalytic H_2 oxidation (Fig. 5 and Fig. S5 in the ESI[†]).^{16,17} The peak current for the catalytic waves, i_{cat} ,

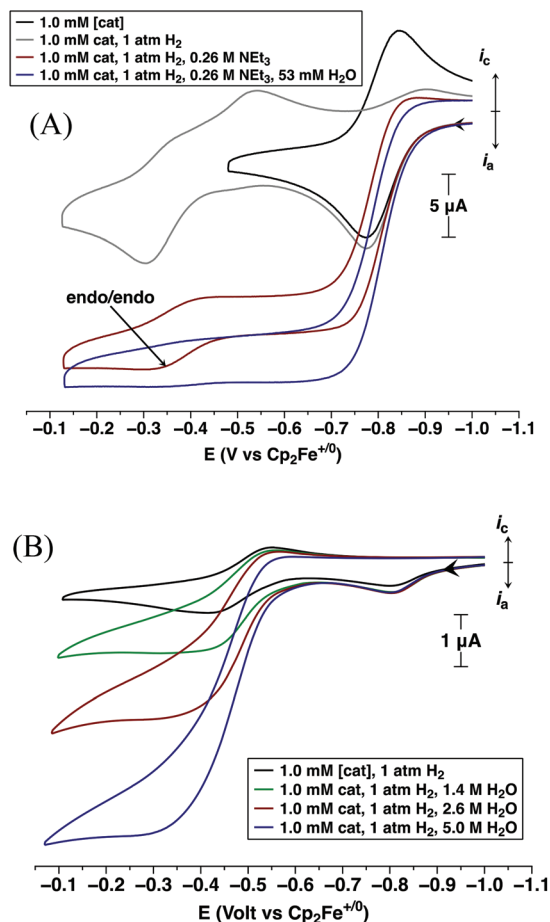


Fig. 5 Cyclic voltammograms of 1.0 mM $[\text{Ni}(\text{P}^{\text{Cy}}_2\text{N}(\text{CH}_2)_2\text{OMe}_2\text{H})_2]^{2+}$ with (A) subsequent additions of NET_3 and H_2O and (B) subsequent additions of H_2O only. Conditions: 0.20 M $[\text{Bu}_4\text{N}][\text{PF}_6]-\text{CH}_3\text{CN}$; 1 mm glassy-carbon working electrode; scan rate (A) 1 V s^{-1} and (B) 0.05 V s^{-1} at 25°C . Note the different operating potentials for the strong vs. the weak base, which indicate a different mechanism of catalysis.

are independent of scan rate between $0.1\text{--}5 \text{ V s}^{-1}$, indicating steady state conditions; however, catalytic wave shapes and plateaus were best defined at a scan rate of 1 V s^{-1} , which was used for calculating the turnover frequencies (k_{obs}). The potential used to calculate the overpotential, $E_{\text{cat}/2}$, is defined as the potential at half of the catalytic current used to calculate k_{obs} ($E_{\text{cat}/2}$, Fig. S4 in the ESI[†]). Turnover frequencies (k_{obs}) were determined from the ratio of i_{cat}/i_p using eqn (5) where n is the number of electrons (2 for H_2 oxidation), R is the gas constant ($8.314 \text{ J K}^{-1} \text{ mol}^{-1}$), F is Faraday's constant ($9.65 \times 10^4 \text{ C mol}^{-1}$), T is the temperature (298 K), and v is the scan rate in V s^{-1} (Table S4 in the ESI[†]).^{18–21} Based on previous studies where water was shown to increase catalytic rates for $[\text{Ni}(\text{P}^{\text{Cy}}_2\text{N}^{\text{R}'}_2)_2](\text{BF}_4)_2$ ($\text{R}' = ^t\text{Bu}, \text{Bn}$ derivatives) complexes when sterically bulky amines were used as the exogenous base, aliquots of purified H_2O were added subsequent to the completion of base additions, resulting in a further catalytic current enhancement (Fig. 5, blue trace).^{8,11} In addition to using amines as strong exogenous bases, H_2O was also used solely as a weak exogenous base. As expected based on

Table 2 Electrocatalytic data for hydrogen oxidation by 1 mM $[\text{Ni}(\text{P}^{\text{Cy}}_2\text{N}^{(\text{CH}_2)_2\text{OMe}}_2)_2]^{2+}$ under 1 atm H_2 in 0.2 M $[\text{Bu}_4\text{N}][\text{PF}_6]-\text{CH}_3\text{CN}$

Exogenous base	$E_{\text{cat}/2}$ (V)	Overpotential (mV)	[Base]	k_{obs} (s^{-1})	[Base], $[\text{H}_2\text{O}]$	k_{obs} (s^{-1})
NEt_3	-0.82	320 ^a	0.26 M	7	0.26 M, 0.05 M	10
^t BuNH ₂	-0.81	290 ^a	0.18 M	13	0.18 M, 0.14 M	17
ⁿ BuNH ₂	-0.81	300 ^a	0.02 M	17	0.02 M, 0.01 M	18
H_2O	-0.48	720 ^b	5.0 M	5	—	—

^a Determined by the method of Evans with the $E_{\text{H}^+/\text{H}_2} = -0.028$ V as determined by Roberts (Fig. S4 in the ESI).^{22,23} ^b Determined by open circuit measurement as previously reported.⁹

previous reports, an alternative mechanism is observed in this case, that entails oxidation of the doubly protonated Ni(0) complex, $[\text{Ni}(\text{P}^{\text{Cy}}_2\text{N}^{(\text{CH}_2)_2\text{OMe}}_2)_2]^{2+}$, before deprotonation.⁸ The calculated turnover frequencies (k_{obs}), overpotentials, conditions and half-peak potentials are reported in Table 2.

$$\frac{i_{\text{cat}}}{i_{\text{p}}} = \frac{n}{0.4463} \sqrt{\frac{RTk_{\text{obs}}}{Fv}} \quad (5)$$

The rate law for the catalytic oxidation of H_2 by $[\text{Ni}(\text{P}^{\text{Cy}}_2\text{N}^{(\text{CH}_2)_2\text{OMe}}_2)_2]^{2+}$ is shown in eqn (6). Using a constant base concentration and measuring i_{cat} as a function of catalyst concentration, the data show a first-order dependence on catalyst concentration (*i.e.* eqn (6), $x = 1$; Fig. S6 in the ESI†). Calcula-

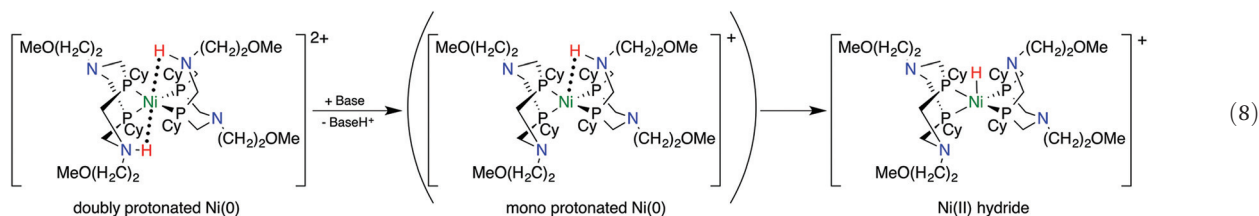
tion of k_{obs} was only done after subsequent base additions resulted in no additional catalytic current enhancement, indicating that pseudo-zero-order conditions with respect to base concentration have been reached (*i.e.* eqn (7), $y = 0$; Fig. S7 in the ESI†). The resulting calculated k_{obs} is a function of k and the H_2 pressure (1 atm).

$$\text{Rate} = k_{\text{obs}}[\text{cat}]^x \quad (6)$$

$$k_{\text{obs}} = k[\text{base}]^y P_{\text{H}_2}^z \quad (7)$$

Thermodynamic studies

Addition of one equivalent of a strong base such as TMG to the doubly protonated Ni(0) isomers of $[\text{Ni}(\text{P}^{\text{Cy}}_2\text{N}^{(\text{CH}_2)_2\text{OMe}}_2)_2]^{2+}$ results in deprotonation to form the mono protonated Ni(0) species that likely undergoes rapid intramolecular isomerization



to form the Ni(II) hydride, $[\text{HNi}(\text{P}^{\text{Cy}}_2\text{N}^{(\text{CH}_2)_2\text{OMe}}_2)]^+$, as monitored by $^{31}\text{P}\{^1\text{H}\}$ NMR spectroscopy (eqn (8), see S8 and S9 in the ESI† for ^1H and ^{31}P NMR spectra).²⁴ Addition of 2,4,6-collidinium ($\text{p}K_{\text{a}} = 15.0$ in acetonitrile) results in an equilibrium mixture of the doubly protonated Ni(0) isomers and the Ni(II) hydride allowing the determination of the effective $\text{p}K_{\text{a}}$ values for the *endo/endo*, *endo/exo* and *exo/exo* isomers of $[\text{Ni}(\text{P}^{\text{Cy}}_2\text{N}^{(\text{CH}_2)_2\text{OMe}}_2)_2]^{2+}$. Using integration of $^{31}\text{P}\{^1\text{H}\}$ NMR spectra to quantify the various nickel species and the ratio of 2,4,6-collidinium to 2,4,6-collidine, the $\text{p}K_{\text{a}}$ of the doubly protonated isomers were determined to be 15.1 (*endo/endo*), 15.2 (*endo/exo*) and 15.4 (*exo/exo*) using the thermodynamic scheme in Fig. 6.

Computational studies

Theoretical calculations have been carried out to investigate the interaction of the methoxyethyl group and the protonated pendant amines in the doubly-protonated isomers of $[\text{Ni}(\text{P}^{\text{Cy}}_2\text{N}^{(\text{CH}_2)_2\text{OMe}}_2)_2]^{2+}$. Calculated $\text{p}K_{\text{a}}$ values and electrochemical

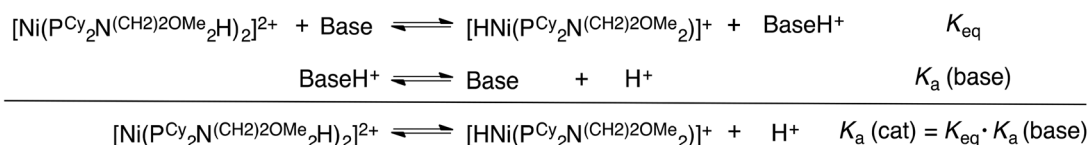


Fig. 6 Thermochemical scheme used for calculating the average $\text{p}K_{\text{a}}$ value of $[\text{Ni}(\text{P}^{\text{Cy}}_2\text{N}^{(\text{CH}_2)_2\text{OMe}}_2)_2]^{2+}$.

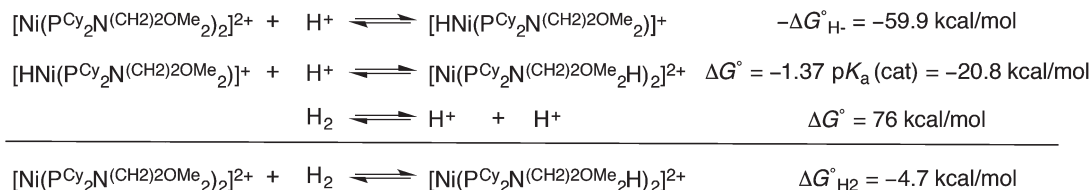


Fig. 7 Thermochemical scheme used for calculating the $\Delta G^\circ_{\text{H}_2}$ of $[\text{Ni}(\text{P}^{\text{Cy}}_2\text{N}(\text{CH}_2)_2\text{OMe}_2\text{H})_2]^{2+}$.²⁶

potentials are reported in Table 1. Additionally, the proposed mechanisms for electrocatalytic oxidation of H_2 using $[\text{Ni}(\text{P}^{\text{Cy}}_2\text{N}(\text{CH}_2)_2\text{OMe}_2)_2]^{2+}$ were also explored computationally.

Hydrogen bonding. The interaction of the methoxyethyl group with the protonated pendant amine in the doubly-protonated Ni(0) *endo/endo*, *endo/exo* and *exo/exo* isomers was explored computationally. The methoxyethyl groups were found to form a weak hydrogen bond with both *endo* and *exo* protonated pendant amines (Fig. 8). The lengths of the O...HN, Ni...HN and N...HN hydrogen bonds are 2.6 Å, 2.6 Å and 1.6 Å, respectively. The O...HN distance is similar for both *endo* and *exo* protons (Fig. 8). The Ni...HN hydrogen bond calculated for the methoxyethyl derivative is slightly longer than that of other Ni catalysts. For example, in $[\text{Ni}(\text{P}^{\text{Cy}}_2\text{N}^{\text{Me}}_2\text{H})_2]^{2+}$, the calculated Ni...HN distance is 2.4 Å.²⁷

Mechanism of catalysis. The proposed CECE mechanism of catalysis (where C represents a chemical deprotonation and E represents an electrochemical oxidation) using strong and weak exogenous bases was investigated through computational analysis of the possible intermediates in the catalytic cycle. Calculated $\text{p}K_{\text{a}}$ values for protonated species and oxidation potentials are reported in Table 1 and Fig. 9 (red). The Ni(0) *endo/endo* isomer was found to have a calculated $\text{p}K_{\text{a}}$ value of 15.3 and an oxidation potential of -0.25 V. In the case of strong exogenous bases (NEt_3 , $^t\text{BuNH}_2$, $^n\text{BuNH}_2$) their $\text{p}K_{\text{a}}$ values (18.1–18.8 are sufficient to allow for deprotonation to form the Ni(0) *endo* isomer (Fig. 9, black CECE pathway). In the case of H_2O as the exogenous base, however, deprotonation

is not favored. The calculated free energy profile for the CECE mechanism using either NEt_3 or H_2O as the exogenous base and a potential of -0.75 V is shown in Fig. 10. Using NEt_3 as the exogenous base results in deprotonation steps that decrease in free energy and an overall ΔG_{rxn} of -11.2 kcal mol⁻¹ (Fig. 10, blue). On the other hand, using H_2O as the exogenous base results in unfavorable deprotonation steps that result in an overall ΔG_{rxn} of $+34.2$ kcal mol⁻¹ (Fig. 10, red). Clearly in the case of H_2O as the exogenous base, the CECE mechanism is not favored. In the case of a strong exogenous base, the rate of H_2 oxidation catalyzed by $[\text{Ni}(\text{P}^{\text{Cy}}_2\text{N}(\text{CH}_2)_2\text{OMe}_2)_2]^{2+}$ is in between that for the $[\text{Ni}(\text{P}^{\text{Cy}}_2\text{N}^{\text{Bn}}_2)_2]^{2+}$ and the $[\text{Ni}(\text{P}^{\text{Cy}}_2\text{N}^{\text{tBu}}_2)_2]^{2+}$ complexes, as expected based on the intermediate $\Delta G^\circ_{\text{H}_2}$.

Discussion

Previous studies have shown that $[\text{Ni}(\text{P}^{\text{R}}_2\text{N}^{\text{R}'}_2)_2]^{2+}$ complexes are very active catalysts for H_2 production and oxidation.² Systematic variations of the R substituents on P and the R' groups on N have been used to control the hydride donor/acceptor ability of the Ni center and the basicity or proton acceptor ability of the pendant base, hence, controlling the free energy of H_2 addition ($\Delta G^\circ_{\text{H}_2}$) to these complexes. We have previously reported that the complex $[\text{Ni}(\text{P}^{\text{Cy}}_2\text{N}^{\text{tBu}}_2)_2]^{2+}$ is a catalyst for hydrogen oxidation, with a turnover frequency as high as 58 s⁻¹ under one atmosphere of H_2 in the presence of $^n\text{BuNH}_2$ and H_2O .^{7,8} In an effort to understand the role of water and potentially increase intra- and intermolecular proton transfer in this class of catalyst, we appended methoxyethyl groups in the outer coordination sphere. To that end, we have synthesized and studied $[\text{Ni}(\text{P}^{\text{Cy}}_2\text{N}(\text{CH}_2)_2\text{OMe}_2)_2]^{2+}$ that contains pendant ether groups in the outer coordination sphere of the metal complex. In addition to being an effective electrocatalyst for H_2 oxidation, this compound shows rapid proton transfer between the three isomers of its H_2 addition products. In this paper, we discuss the differences in the H_2 oxidation properties of $[\text{Ni}(\text{P}^{\text{Cy}}_2\text{N}(\text{CH}_2)_2\text{OMe}_2)_2]^{2+}$ compared to the previously reported $[\text{Ni}(\text{P}^{\text{Cy}}_2\text{N}^{\text{R}'}_2)_2]^{2+}$ catalysts.^{8–11}

The reaction of $[\text{Ni}(\text{P}^{\text{Cy}}_2\text{N}(\text{CH}_2)_2\text{OMe}_2)_2]^{2+}$ with H_2 results in the formation of the doubly protonated Ni(0) product that exists in the form of three isomers, *endo/endo*, *endo/exo*, and *exo/exo* (Scheme 1) in the time it takes to prepare the sample and collect the data (<15 min.). Similar isomers have been reported previously in the reaction of other complexes of this type with H_2 , and their structures were deduced by extensive ^1H , ^{31}P , and ^{15}N NMR studies.^{7,8,11,15} The kinetic product of

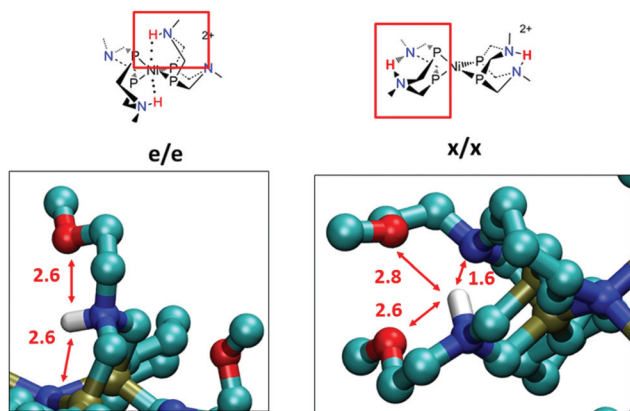


Fig. 8 The structural characteristics of the hydrogen bond network around the pendant amines in Ni(0) *endo/endo* and *exo/exo* isomers of $[\text{Ni}(\text{P}^{\text{Cy}}_2\text{N}(\text{CH}_2)_2\text{OMe}_2)_2]^{2+}$. Distances in Å are shown in red.

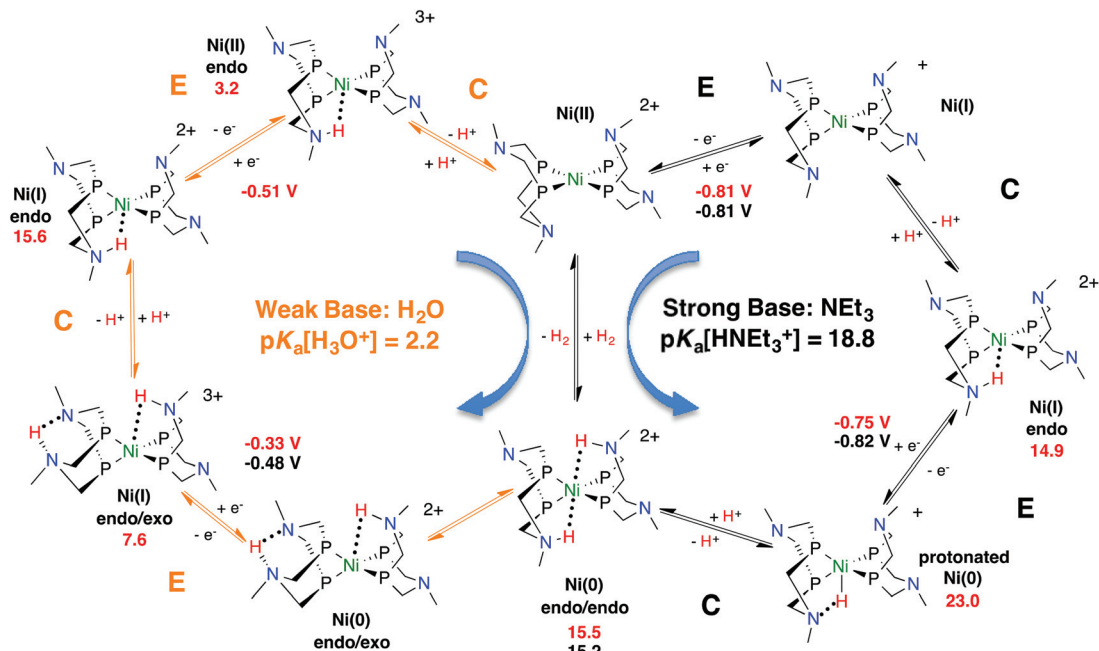


Fig. 9 Proposed mechanism for the electrocatalytic oxidation of H₂ with [Ni(P(Cy₂N(CH₂)₂OMe)₂)₂]²⁺ showing the CECE pathway (black arrows, counterclockwise) and the ECEC pathway (orange arrows, clockwise). Experimental (black) and computational values (red) for the oxidation potentials and pK_a values are shown. The substituents on the phosphorus and nitrogen atoms were omitted for clarity.

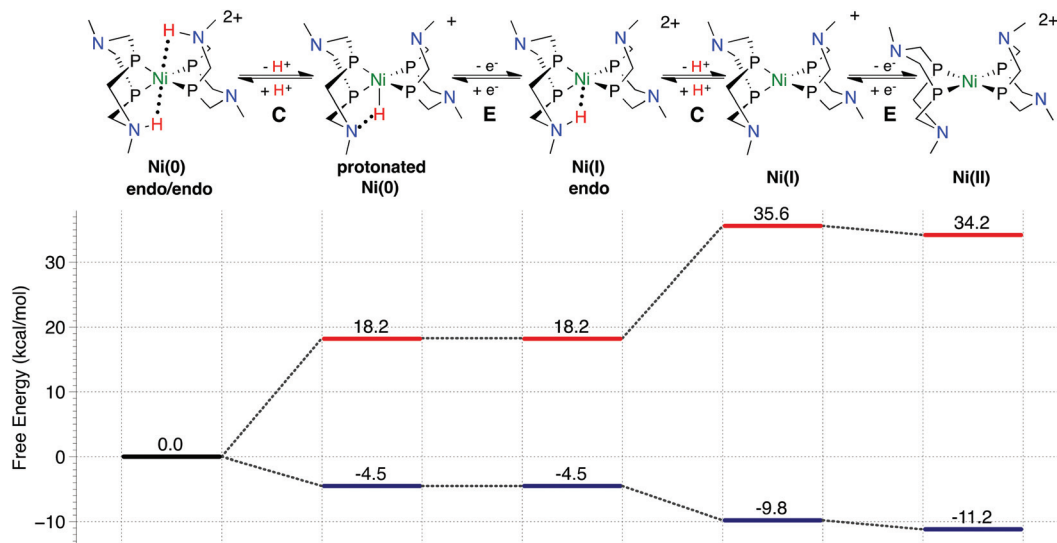


Fig. 10 Calculated free energy profile at -0.75 V for the CECE mechanism for catalytic H₂ oxidation with [Ni(P(Cy₂N(CH₂)₂OMe)₂)₂]²⁺ using NEt₃ (blue) or H₂O (red) as the exogenous bases.

addition of H₂ to [Ni(P(Cy₂N(CH₂)₂OMe)₂)₂]²⁺ is the *endo/endo* isomer, which has both protons *endo* with respect to the metal, as established in the previously studied [Ni(P(Cy₂N(R')₂)₂)₂]²⁺ (R' = Bn, Bn derivatives, ^tBu).^{7–10} The *endo/endo* isomer then undergoes intermolecular deprotonation and reprotonation to form the *endo/exo* and *exo/exo* isomers. In the case of [Ni(P(Cy₂N(R')₂)₂)₂]²⁺ (R' = Bn or ^tBu) the rate of this isomerization process to reach equilibrium is slow (>10 h). However, the

addition of water or exogenous base facilitates the intermolecular exchange, resulting in a more rapid approach to equilibrium (<5 h).²⁴ In the case of [Ni(P(Cy₂N(3-pyridazyl)methyl)₂)₂]²⁺ the isomerization process is extremely fast, occurring in less than 15 min. at room temperature, without the addition of water, attributed to the additional bases in the outer coordination sphere.⁹ The similar fast isomerization observed here in the absence of water indicates that the additional pendant groups

in the case of $[\text{Ni}(\text{P}^{\text{Cy}}_2\text{N}^{(\text{CH}_2)_2\text{OMe}}_2)_2]^{2+}$ are facilitating rapid proton movement similar to $[\text{Ni}(\text{P}^{\text{Cy}}_2\text{N}^{(3\text{-pyridazyl)methyl}}_2)_2]^{2+}$. Isomerization studies carried out at 0 °C with $[\text{Ni}(\text{P}^{\text{Cy}}_2\text{N}^{(\text{CH}_2)_2\text{OMe}}_2)_2]^{2+}$ and H_2 at different catalyst concentrations suggest the rate-determining step of the isomerization is likely an intramolecular process. This is in stark contrast to the intermolecular exchange process observed for the $[\text{Ni}(\text{P}^{\text{Cy}}_2\text{N}^{\text{R}}_2\text{H})_2]^{2+}$ ($\text{R} = \text{Bn}$ or ^tBu) derivatives, providing further evidence that the pendant ether group plays a role in the isomerization process for $[\text{Ni}(\text{P}^{\text{Cy}}_2\text{N}^{(\text{CH}_2)_2\text{OMe}}_2\text{H})_2]^{2+}$.¹⁴ While the rate of proton movement does not influence catalysis for this complex, understanding the movement of protons from the active site may be essential as the rates of catalysis become faster.

An interaction of the methoxyethyl group with the *endo* protons in the doubly protonated Ni(0) isomers of the $[\text{Ni}(\text{P}^{\text{Cy}}_2\text{N}^{(\text{CH}_2)_2\text{OMe}}_2\text{H})_2]^{2+}$ complex is also suggested by the distribution of isomers at equilibrium. A significantly higher population of *exo/exo* species is observed ($\approx 50\%$) compared to the $[\text{Ni}(\text{P}^{\text{Cy}}_2\text{N}^{\text{R}}_2\text{H})_2]^{2+}$ ($\text{R} = \text{Bn}$ or ^tBu) derivatives ($\approx 10\%$), indicative a weakened *endo* Ni...HN hydrogen bond.^{7,14} The same effect was also observed for the complex with an appended pyridazine in the outer coordination sphere.⁹ The negatively shifted potentials for the doubly protonated isomers as compared to $[\text{Ni}(\text{P}^{\text{Cy}}_2\text{N}^{\text{Bn}}_2\text{H})_2]^{2+}$ are also suggestive of this interpretation.^{9,28} This was characterized computationally and the Ni...HN hydrogen bond was found to be slightly longer, lowering the barrier associated for the isomerization reaction, as also seen in previous systems containing outer coordination sphere pendant groups.^{9,11} In contrast, the N...HN bond in *exo* positions is of similar length and energy computationally observed for other systems, indicating that hydrogen bonding with the methoxyethyl moiety has little effect on the *exo* pinched hydrogen bond.²⁷ The computational data corroborates that the fast rates for isomerization observed in formation of the isomers of $[\text{Ni}(\text{P}^{\text{Cy}}_2\text{N}^{(\text{CH}_2)_2\text{OMe}}_2\text{H})_2]^{2+}$ is likely due to the appended basic groups that are not present in the $[\text{Ni}(\text{P}^{\text{Cy}}_2\text{N}^{\text{Bn}}_2)_2]^{2+}$ and $[\text{Ni}(\text{P}^{\text{Cy}}_2\text{N}^{^t\text{Bu}}_2)_2]^{2+}$ compounds.

The cyclic voltammograms of the *endo/endo*, *endo/exo* and *exo/exo* isomers of $[\text{Ni}(\text{P}^{\text{Cy}}_2\text{N}^{(\text{CH}_2)_2\text{OMe}}_2\text{H})_2]^{2+}$ (Scheme 1) show different oxidation potentials, illustrated in Fig. 4 and compiled in Table 1, as previously reported for the $[\text{Ni}(\text{P}^{\text{Cy}}_2\text{N}^{\text{R}'}_2)_2]^{2+}$ ($\text{R}' = \text{Bn}$, Bn derivatives, ^tBu and (3-pyridazyl)methyl) and $[\text{Ni}(\text{P}^{\text{Cy}}_2\text{N}^{\text{Bn}}_2)_2]^{2+}$ compounds.^{2,8,9,11,28} Each of the isomers has two hydrogen bonds consisting of either N...HN or Ni...HN hydrogen bonds (Scheme 1). The differences in oxidation potentials for the three isomers is likely due to the difference in the nature of the hydrogen bonding.²⁸ The Ni...HN hydrogen bonds stabilize the HOMO of the Ni(0), which results in a higher oxidation potential for the metal in the *endo/endo* isomer. In the previously reported $[\text{Ni}(\text{P}^{\text{Cy}}_2\text{N}^{(3\text{-pyridazyl)methyl}}_2)_2]^{2+}$ compound the additional pendant amine in the outer coordination sphere is thought to destabilize the Ni...HN hydrogen bond through formation of an N...HN hydrogen bond from the nitrogen to the pendant amine.⁹ As shown by the computational work, a similar effect is thought to be occurring in the *endo/endo* isomer of

$[\text{Ni}(\text{P}^{\text{Cy}}_2\text{N}^{(\text{CH}_2)_2\text{OMe}}_2\text{H})_2]^{2+}$; the Ni...HN hydrogen bond is destabilized through formation of an O...HN hydrogen bond from the outer pendant ether group.⁹ The weakening of the hydrogen bonds results in a 150 mV lower overpotential for $[\text{Ni}(\text{P}^{\text{Cy}}_2\text{N}^{(\text{CH}_2)_2\text{OMe}}_2)_2]^{2+}$ than for $[\text{Ni}(\text{P}^{\text{Cy}}_2\text{N}^{\text{Bn}}_2)_2]^{2+}$ when a weak exogenous base is used for catalysis.

The mechanism for the electrocatalytic oxidation of H_2 by $[\text{Ni}(\text{P}^{\text{R}}_2\text{N}^{\text{R}'}_2)_2]^{2+}$ compounds has been thoroughly studied both experimentally and computationally.^{10,27} Catalytic oxidation of H_2 by $[\text{Ni}(\text{P}^{\text{Cy}}_2\text{N}^{(\text{CH}_2)_2\text{OMe}}_2)_2]^{2+}$ proceeds by two different catalytic pathways consisting of chemical (C) and electrochemical (E) steps depending on the steric size, strength and nature of the exogenous base, as noted previously.⁸ In the case of a strong exogenous base, deprotonation proceeds before oxidation (Fig. 9, black CECE pathway) and catalysis occurs at more negative potentials.⁸ In contrast, when a weak exogenous base is used, oxidation of the doubly protonated Ni(0) isomers must occur before intermolecular deprotonation (Fig. 9, orange ECEC pathway). Although the first two steps (EC) of this mechanism were previously reported, the following order of deprotonation and oxidation steps was not established.^{8,9,11} Using computational analysis, we have identified that when a weak exogenous base is used, oxidation occurs before deprotonation in both steps (Fig. 9, orange ECEC pathway). After the first oxidation and deprotonation, the calculated pK_a of the Ni(I) isomer was found to be 15.6, too low in acidity for deprotonation by water, requiring oxidation to the more acidic mono protonated Ni(II) *endo* isomer first. Additionally, the calculated oxidation potential of the mono protonated Ni(I) *endo* isomer is -0.51 V, slightly negative of the operating potential for catalysis (-0.47), indicating oxidation will proceed readily upon its formation. The final step is a deprotonation, which is nearly thermoneutral for water molecule based on the calculated pK_a of the Ni(II) *endo* isomer of 3.2, resulting in the starting Ni(II) complex. Thus the computational result supports the ECEC mechanism.

Conclusions

The $[\text{Ni}(\text{P}^{\text{Cy}}_2\text{N}^{(\text{CH}_2)_2\text{OMe}}_2)_2]^{2+}$ complex has been shown to be an electrocatalyst for the oxidation of H_2 . The pendant methoxy pendant group on the ligand in the outer coordination sphere of the metal complex facilitates isomerization of the H_2 addition product, $[\text{Ni}(\text{P}^{\text{Cy}}_2\text{N}^{(\text{CH}_2)_2\text{OMe}}_2\text{H})_2]^{2+}$. The increase in the rate of isomerization is attributed to a weakening of the Ni(0)...HN hydrogen bond by the methoxy group, consequently lowering the overpotential for H_2 oxidation catalysis. Importantly, the rate of catalysis was faster than the $[\text{Ni}(\text{P}^{\text{Cy}}_2\text{N}^{\text{Bn}}_2)_2]^{2+}$ complex, demonstrating that the methoxyethyl provided both an additional driving force for H_2 addition and an advantageous interaction of the appended ether group to lower the overpotential. Although the $[\text{Ni}(\text{P}^{\text{Cy}}_2\text{N}^{(\text{CH}_2)_2\text{OMe}}_2)_2]^{2+}$ complex operates at a higher overpotential than the pyridazyl complex; the rate is ~ 10 times faster, indicating competitive binding of

the outer coordination group to the Ni(II) center has been avoided. The mechanism with a weak base was investigated computationally and shown to occur through an ECEC mechanism, an important advancement in our understanding of electrocatalytic H₂ oxidation using water as an exogenous base. Work continues in our laboratories on understanding the roles pendant groups in the second and outer coordination spheres of molecular electrocatalysis play in proton movement.

Experimental section

General experimental procedures

All chemicals were purchased from Aldrich and used without any further purification. Solvents were purified by passage through neutral alumina using an Innovative Technology, Inc., PureSolv™ solvent purification system. Decamethylcobaltocenium tetrafluoroborate ([CoCp₂⁺](BF₄)) was purchased from Strem Chemicals Inc. (Newburyport, MA). Deuterated solvents were purchased from Cambridge Isotope Laboratories Inc. (Andover, MA). CD₃CN and CD₂Cl₂ were dried from P₂O₅ and CaH₂, respectively. Ultra-high purity H₂ (99.9%) was from OXARC Inc. (Spokane, WA) and dried using an oxygen trap (Oxy-Purge™ N) from Alltech Associates (Deerfield, IL) and a moisture trap (Model MT-4-S) from Agilent Technologies (Santa Clara, CA). All manipulations and chemical reactions were performed either under a nitrogen atmosphere using standard Schlenk line or inert atmosphere glove box techniques. Bis(hydroxymethyl)cyclohexylphosphine (CyP(CH₂OH)₂) was synthesized according to the published procedure.⁷ Elemental analyses were performed at Atlantic Micro-lab Inc. (Norcross, GA).

Instrumentation

¹H and ³¹P{¹H} NMR measurements were carried out in Varian Inova or VNMRs spectrometer (500 MHz for ¹H NMR, 200 MHz for ³¹P NMR). Proton resonances were internally calibrated to the residual ¹H signals from the deuterated solvents, while ³¹P resonances were calibrated against 85% H₃PO₄ (external standard).

Electrochemical measurements were carried out using a CH Instruments 660D potentiostat equipped with a standard three-electrode cell. Prior to the collection of each cyclic voltammogram (CV), the working electrode (1 mm PEEK-encased glassy carbon, Cypress Systems EE040) was polished using the diamond paste (Buehler). A 3-mm glassy carbon rod (Alfa) was used as the counter-electrode, and a silver wire suspended in the electrolyte solution and separated from the analyte solution by a Vycor frit (CH Instruments 112) was used as a reference electrode. Electrochemical measurements were carried out either under N₂ or H₂ in an anaerobic glove box and a 0.2 M solution of tetrabutylammonium hexafluorophosphate in acetonitrile was used as an electrolyte. [CoCp₂⁺](BF₄) was used as an internal standard for hydrogen oxidation reactions

and the cyclic voltammograms were referenced to the ferrocene/ferrocenium couple at 0.0 V.

Computational details

The structure of the species discussed in the paper was optimized without symmetry constraints within the density functional theory framework using the B3P86 exchange and correlation functional.^{29,30} The Stuttgart basis set with effective core potential was used for Ni atom, whereas the 6-31G* basis set was used for all of the other atoms with one additional *p* polarization function for the proton on pendant amines. The optimized structures were confirmed by frequency calculations. Harmonic vibrational frequencies were calculated at the optimized geometries using the same level of theory to estimate the zero-point energy (ZPE) and the thermal contributions (298 K and 1 atm) to the gas-phase free energy. Free energies of solvation in acetonitrile (which include the change of thermodynamic conditions of *P* = 1 atm in the gas phase to 1 M solution) were then computed using a self-consistent reaction field (SCRF) model at the same level of theory as for the other steps. The conductor-like polarizable continuum model (CPCM)^{31,32} was used with Bondi radii.³³ The p*K*_a values and redox potential were calculated according to the isodesmic scheme discussed by Chen *et al.*³⁴ The [Ni(P^{Cy}₂N^{Bn}₂H_n)₂]²⁺ complex was used as reference for the both p*K*_a and for redox potential calculations. All of the calculations were carried out with the program Gaussian 09.³⁵

Ni(P^{Cy}₂N^{(CH₂)₂OMe₂)₂. CyP(CH₂OH)₂ (4.11 g, 23 mmol) was added to a 250 mL Schlenk flask and dissolved in 60 mL of ethanol. The mixture was heated to 70 °C, then 2-methoxyethylamine (1.75 g, 23 mmol) was added dropwise and the resulting mixture was stirred overnight at 70 °C. Solvents were removed by vacuum to yield a white sticky oil, which was used without further purification. Crude P^{Cy}₂N^{(CH₂)₂OMe₂}, ³¹P{¹H} NMR (Ethanol, 202.2 MHz) δ -40.13 (br). Approximately 30 mL of acetonitrile and 10 mL of tetrahydrofuran (THF) solution was used to dissolve the oil, following which 2.75 g (5.7 mmol) of [Ni(CH₃CN)₆](BF₄)₂ dissolved in a minimum amount of acetonitrile was added and the combined mixture was stirred overnight. The resulting dark-red solution was sparged with H₂ for 30 minutes. Following H₂ sparging, 1,1,3,3-tetramethylguanidine (TMG) (1.44 mL, 11.5 mmol) was added with continuous bubbling of H₂, upon which yellowish-white solids were observed at the bottom of the flask. After cooling to 0 °C overnight, a pale yellow solid of pure Ni-(P^{Cy}₂N^{(CH₂)₂OMe₂)₂ was isolated after filtration and washing with cold CH₃CN. Yield 1.17 g (22%). ³¹P{¹H} NMR (C₆D₆, 121.0 MHz): δ 9.47 (s). ¹H NMR (C₆D₆, 299.9 MHz): δ 3.60 (t, 8H, NCH₂CH₂OMe), 3.22 (s, 12H, NCH₂CH₂OCH₃), 2.95 (t, 8H, NCH₂CH₂OMe), 2.86 (d, 8H, PCH₂), 2.65 (d, 8H, PCH₂), 1.86 (d, 8H, CyH), 1.76 (d, 12H, CyH), 1.64 (d, 8H, CyH), 1.10–1.50 (multiple peaks, 16H, CyH). Anal. calcd (found) for Ni(P^{Cy}₂N^{(CH₂)₂OMe₂)₂ C₄₄H₈₈N₄NiO₄P₄%C 57.46 (56.32), %H 9.67 (9.64), %N 5.97 (6.09).}}}}

[Ni(P^{Cy}₂N^{(CH₂)₂OMe₂)₂](BF₄)₂. To 0.237 g of Ni(P^{Cy}₂N^{(CH₂)₂OMe₂)₂ (0.258 mmol) dissolved in 2 mL of CH₃CN, 0.140 g}}

(0.516 mmol) of decamethylferrocenium tetrafluoroborate ($\text{Cp}_2^+\text{Fe}\text{BF}_4$) dissolved in 2 mL of CH_3CN was added and stirred overnight. The reaction solution was concentrated until the precipitation of ferrocene began then stored overnight in a $-35\text{ }^\circ\text{C}$ freezer. The mother liquor was then extracted with a pipette and the remaining solid was washed with 2 mL of cold acetonitrile and dried under vacuum. The isolated solid was dissolved in CH_3CN and layered with diethyl ether resulting in precipitation of a red solid. Yield 0.266 g (95%). $^{31}\text{P}\{^1\text{H}\}$ NMR (CD_3CN , 202.2 MHz): δ 8.21 (s). ^1H NMR (CD_3CN , 499.9 MHz): δ 3.54 (br, 8H, $\text{NCH}_2\text{CH}_2\text{OMe}$), 3.30 (s, 12H, $\text{NCH}_2\text{CH}_2\text{OCH}_3$), 3.18 (d, 8H, $\text{NCH}_2\text{CH}_2\text{OMe}$), 3.10 (d, 4H, PCH_2), 2.89 (br, 8H, PCH_2), 2.80 (br, 4H, PCH_2), 1.86 (d, 8H, CyH), 1.76 (d, 12H, CyH), 1.60–2.10 (multiple peaks, 24H, CyH), 1.10–1.50 (br, 20H, CyH). Anal. calcd (found) for $[\text{Ni}(\text{P}^{\text{Cy}}_2\text{N}^{(\text{CH}_2)_2\text{OMe}}_2)]\text{-(BF}_4)_2 \cdot 0.5\text{CH}_2\text{Cl}_2$ $\text{C}_{44.5}\text{H}_{89}\text{B}_2\text{ClF}_8\text{N}_4\text{NiO}_4\text{P}_4$ %C 47.05 (47.22), %H 7.90 (7.83), %N 4.93 (5.21), %F 13.38 (13.56). The presence of 0.5 equivalent of dichloromethane was confirmed by the ^1H NMR spectra in CD_3CN .

NMR experiments

In a typical H_2 addition experiment, 15 mg (0.014 mmol) of $[\text{Ni}(\text{P}^{\text{Cy}}_2\text{N}^{(\text{CH}_2)_2\text{OMe}}_2)]\text{-(BF}_4)_2$ was dissolved in CD_3CN and hydrogen gas was sparged into the solution for five minutes. The resulting solution containing $[\text{Ni}(\text{P}^{\text{Cy}}_2\text{N}^{(\text{CH}_2)_2\text{OMe}}_2\text{H})]^{2+}$ was analyzed by $^{31}\text{P}\{^1\text{H}\}$ NMR spectroscopy. The *endo/endo* and *exo/exo* isomers showed peaks at 18.6 and -10.1 ppm, respectively in the $^{31}\text{P}\{^1\text{H}\}$ NMR spectrum at room temperature. The *endo/exo* isomer (B) showed peaks at 17.8 and -9.0 ppm. The peak integration was done by using the VNMRJ software from Agilent Technologies (Santa Clara, CA).

Determination of the rate of equilibration of the isomers below room temperature was performed using a sample that was maintained at $0\text{ }^\circ\text{C}$. The Ni(II) complex was dissolved in CD_3CN and immersed into a $0\text{ }^\circ\text{C}$ cold bath. The solution was sparged with hydrogen gas for 5 minutes. Data were collected on an NMR spectrometer with the probe precooled and maintained at $0\text{ }^\circ\text{C}$ for ≈ 6 h. The rate of formation of the *exo/exo* isomer was obtained by plotting the integrated area of the peak at -10 ppm in the $^{31}\text{P}\{^1\text{H}\}$ NMR spectrum *versus* time. The reaction was repeated at three different concentrations (20, 10, and 5 mM) and each concentration was repeated twice.

NMR correlation experiments

Homonuclear exchange correlation experiment (^{31}P -EXSY) was performed in VNMRJ 500 MHz spectrometer, using a standard 2D-VNMRJ pulse sequence with 256 increments, 64 scans per increments, and 200 ms mixing time (for the $40\text{ }^\circ\text{C}$ experiment). In addition, ^{31}P -EXSY spectra were recorded at varying temperatures: -40 , 0 , 25 and $40\text{ }^\circ\text{C}$.

Catalytic hydrogen oxidation

A typical electrocatalytic H_2 oxidation experiment was started from the Ni(I) complex $[\text{Ni}(\text{P}^{\text{Cy}}_2\text{N}^{(\text{CH}_2)_2\text{OMe}}_2)]^+$, which was generated *in situ* by reacting the Ni(II) complex $[\text{Ni}(\text{P}^{\text{Cy}}_2\text{N}^{(\text{CH}_2)_2\text{OMe}}_2)]^{2+}$

(0.164 mg, $1.5\text{ }\mu\text{mol}$) and the Ni(0) complex $\text{Ni}(\text{P}^{\text{Cy}}_2\text{N}^{(\text{CH}_2)_2\text{OMe}}_2)_2$ (0.137 mg, $1.5\text{ }\mu\text{mol}$) in 3 mL of acetonitrile. A portion (2 mL) of this solution was placed into the electrochemistry cell. A small amount of decamethylcobaltocenium tetrafluoroborate ($E^\circ \text{CoCp}^{*2+/0} = -1.895\text{ V vs. FeCp}^{+/0}$) was added as an internal standard. Hydrogen gas was sparged through the solution for 5 minutes and the needle was placed above the solution to maintain a constant pressure of hydrogen before measuring the cyclic voltammograms, which were collected at scan rates of 50 mV s^{-1} to 10 V s^{-1} . The working electrode was polished using the diamond paste (Buehler) and thoroughly cleaned and rinsed with acetonitrile. Base and water were added using a micropipette or syringe.

Acknowledgements

We thank Dr Jonathan Darmon for providing the cover artwork. This research was supported as part of the Center for Molecular Electrocatalysis, an Energy Frontier Research Center funded by the U.S. Department of Energy, Office of Science, Office of Basic Energy Sciences. Pacific Northwest National Laboratory is operated by Battelle for the U.S. Department of Energy.

References

- 1 *Catalysis without Precious Metals*, ed. R. M. Bullock, Wiley-VCH, 1st edn, 2010.
- 2 W. J. Shaw, M. L. Helm and D. L. DuBois, *Biochim. Biophys. Acta, Bioenerg.*, 2013, **1827**, 1123–1139.
- 3 V. S. Thoi, Y. Sun, J. R. Long and C. J. Chang, *Chem. Soc. Rev.*, 2013, **42**, 2388–2400.
- 4 A. Jain, M. L. Reback, M. L. Lindstrom, C. E. Thogerson, M. L. Helm, A. M. Appel and W. J. Shaw, *Inorg. Chem.*, 2012, **51**, 6592–6602.
- 5 M. L. Reback, B. Ginovska-Pangovska, M.-H. Ho, A. Jain, T. C. Squier, S. Raugei, J. A. S. Roberts and W. J. Shaw, *Chem.-Eur. J.*, 2012, **19**, 1928–1941.
- 6 N. Wang, M. Wang, Y. Wang, D. Zheng, H. Han, M. S. G. Ahlquist and L. Sun, *J. Am. Chem. Soc.*, 2013, **135**, 13688–13691.
- 7 J. Y. Yang, S. Chen, W. G. Dougherty, W. S. Kassel, R. M. Bullock, D. L. DuBois, S. Raugei, R. J. Rousseau, M. Dupuis and M. Rakowski DuBois, *Chem. Commun.*, 2010, **46**, 8618–8620.
- 8 J. Y. Yang, S. E. Smith, T. Liu, W. G. Dougherty, W. A. Hoffert, W. S. Kassel, M. Rakowski DuBois, D. L. DuBois and R. M. Bullock, *J. Am. Chem. Soc.*, 2013, **135**, 9700–9712.
- 9 S. Lense, J. A. S. Roberts and W. J. Shaw, *Chem. Commun.*, 2013, 1–3.
- 10 A. D. Wilson, R. H. Newell, M. J. McNevin, J. T. Muckerman, M. Rakowski DuBois and D. L. DuBois, *J. Am. Chem. Soc.*, 2006, **128**, 358–366.

- 11 S. Lense, M.-H. Ho, S. Chen, A. Jain, S. Raugei, J. C. Linehan, J. A. S. Roberts, A. M. Appel and W. J. Shaw, *Organometallics*, 2012, **31**, 6719–6731.
- 12 M. R. Ringenberg, M. J. Nilges, T. B. Rauchfuss and S. R. Wilson, *Organometallics*, 2010, **29**, 1956–1965.
- 13 M. R. Ringenberg, S. L. Kokatam, Z. M. Heiden and T. B. Rauchfuss, *J. Am. Chem. Soc.*, 2008, **130**, 788–789.
- 14 M. J. O'Hagan, M.-H. Ho, J. Y. Yang, A. M. Appel, M. Rakowski DuBois, S. Raugei, W. J. Shaw, D. L. DuBois and R. M. Bullock, *J. Am. Chem. Soc.*, 2012, **134**, 19409–19424.
- 15 A. D. Wilson, R. K. Shoemaker, A. Miedaner, J. T. Muckerman, D. L. DuBois and M. Rakowski DuBois, *Proc. Natl. Acad. Sci. U. S. A.*, 2007, **104**, 6951–6956.
- 16 K. Izutsu, *Acid-Base Dissociation Constants in Dipolar Aprotic Solvents*, Blackwell Scientific Publications, 1990.
- 17 I. Kaljurand, A. Kütt, L. Sooväli, T. Rodima, V. Mäemets, I. Leito and I. A. Koppel, *J. Org. Chem.*, 2005, **70**, 1019–1028.
- 18 J. M. Savéant, *Acc. Chem. Res.*, 1980, **13**, 323–329.
- 19 J. M. Savéant and E. Vianello, *Electrochim. Acta*, 1965, **10**, 905–920.
- 20 J. M. Savéant and E. Vianello, *Electrochim. Acta*, 1967, **12**, 629–646.
- 21 R. S. Nicholson, *Anal. Chem.*, 1965, **37**, 1351–1355.
- 22 G. A. N. Felton, R. S. Glass, D. L. Lichtenberger and D. H. Evans, *Inorg. Chem.*, 2006, **45**, 9181–9184.
- 23 J. A. S. Roberts and R. M. Bullock, *Inorg. Chem.*, 2013, **52**, 3823–3835.
- 24 M. J. O'Hagan, W. J. Shaw, S. Raugei, S. Chen, J. Y. Yang, U. J. Kilgore, D. L. DuBois and R. M. Bullock, *J. Am. Chem. Soc.*, 2011, **133**, 14301–14312.
- 25 B. R. Galan, J. Schöffel, J. C. Linehan, C. Seu, A. M. Appel, J. A. S. Roberts, M. L. Helm, U. J. Kilgore, J. Y. Yang, D. L. DuBois and C. P. Kubiak, *J. Am. Chem. Soc.*, 2011, **133**, 12767–12779.
- 26 C. J. Curtis, A. Miedaner, W. W. Ellis and D. L. DuBois, *J. Am. Chem. Soc.*, 2002, **124**, 1918–1925.
- 27 S. Raugei, S. Chen, M.-H. Ho, B. Ginovska-Pangovska, R. J. Rousseau, M. Dupuis, D. L. DuBois and R. M. Bullock, *Chem.-Eur. J.*, 2012, **18**, 6493–6506.
- 28 E. S. Wiedner, J. Y. Yang, S. Chen, S. Raugei, W. G. Dougherty, W. S. Kassel, M. L. Helm, R. M. Bullock, M. Rakowski DuBois and D. L. DuBois, *Organometallics*, 2012, **31**, 144–156.
- 29 J. P. Perdew, *Phys. Rev. B: Condens. Matter*, 1986, **33**, 8822–8824.
- 30 A. D. Becke, *J. Chem. Phys.*, 1993, **98**, 5648.
- 31 M. Cossi, N. Rega, G. Scalmani and V. Barone, *J. Comput. Chem.*, 2003, **24**, 669–681.
- 32 V. Barone and M. Cossi, *J. Phys. Chem. A*, 1998, **102**, 1995–2001.
- 33 A. Bondi, *J. Phys. Chem.*, 1964, **68**, 441–451.
- 34 S. Chen, R. J. Rousseau, S. Raugei, M. Dupuis, D. L. DuBois and R. M. Bullock, *Organometallics*, 2011, **30**, 6108–6118.
- 35 M. J. Frisch, G. W. Trucks, H. B. Schlegel, G. E. Scuseria, M. A. Robb, J. R. Cheeseman, G. Scalmani, V. Barone, B. Mennucci, G. A. Petersson, H. Nakatsuji, M. Caricato, X. Li, H. P. Hratchian, A. F. Izmaylov, J. Bloino, G. Zheng, J. L. Sonnenberg, M. Hada, M. Ehara, K. Toyota, R. Fukuda, J. Hasegawa, M. Ishida, T. Nakajima, Y. Honda, O. Kitao, H. Nakai, T. Vreven, J. A. Montgomery, J. E. Peralta, F. Ogliaro, M. Bearpark, J. J. Heyd, E. Brothers, K. N. Kudin, V. N. Staroverov, R. Kobayashi, J. Normand, K. Raghavachari, A. Rendell, J. C. Burant, S. S. Iyengar, J. Tomasi, M. Cossi, N. Rega, J. M. Millam, M. Klene, J. E. Knox, J. B. Cross, V. Bakken, C. Adamo, J. Jaramillo, R. Gomperts, R. E. Stratmann, O. Yazyev, A. J. Austin, R. Cammi, C. Pomelli, J. W. Ochterski, R. L. Martin, K. Morokuma, V. G. Zakrzewski, G. A. Voth, P. Salvador, J. J. Dannenberg, S. Dapprich, A. D. Daniels, Ö. Farkas, J. B. Foresman, J. V. Ortiz, J. Cioslowski and D. J. Fox, *GAUSSIAN 09 (Revision B 01)*, Gaussian, Inc, Wallingford, CT, 2009.